

NoRMCorre: An online algorithm for piecewise rigid motion correction of calcium imaging data

Eftychios A. Pnevmatikakis^{a,*}, Andrea Giovannucci^a

^a*Center for Computational Biology, Flatiron Institute, Simons Foundation, New York, NY, USA.*

Abstract

Background: Motion correction is a challenging pre-processing problem that arises early in the analysis pipeline of calcium imaging data sequences. The motion artifacts in two-photon microscopy recordings can be non-rigid, arising from the finite time of raster scanning and non-uniform deformations of the brain medium.

New method: We introduce an algorithm for fast Non-Rigid Motion Correction (NoRMCorre) based on template matching. NoRMCorre operates by splitting the field of view into overlapping spatial patches that are registered at a sub-pixel resolution for rigid translation against a continuously updated template. The estimated alignments are subsequently up-sampled to create a smooth motion field for each frame that can efficiently approximate non-rigid motion in a piecewise-rigid manner.

Existing methods: Existing approaches either do not scale well in terms of computational performance or are targeted to motion artifacts arising from low speed scanning, whereas modern datasets with large field of view are more prone to non-rigid brain deformation issues.

Results: NoRMCorre can be run in an online mode resulting in comparable to or even faster than real time motion registration on streaming data. We evaluate

*Corresponding author

Email address: epnevmatikakis@simonsfoundation.org (Eftychios A. Pnevmatikakis)

the performance of the proposed method with simple yet intuitive metrics and compare against other non-rigid registration methods on two-photon calcium imaging datasets. Open source Matlab and Python code is also made available.

Conclusions: The proposed method and code provide valuable support to the community for solving large scale image registration problems in calcium imaging, especially when non-rigid deformations are present in the acquired data.

Keywords: calcium imaging, motion correction, image registration

2010 MSC: 00-01, 99-00

1 **1. Introduction**

2 Calcium imaging methods enable the monitoring of large neural populations
3 over long periods of time with single neuron resolution. Before addressing spe-
4 cific scientific questions, the analyst needs to pre-process the data and extract
5 the neural signals of interest from the fluorescent microscopy time series im-
6 ages/volumes. The typical calcium imaging pre-processing pipeline consists first
7 of motion correction/image registration of the time series, followed by source
8 extraction, where the different neurons and processes along with their neural ac-
9 tivity time series are extracted. In this paper we focus on the motion correction
10 pre-processing step: we introduce an algorithm for Non-Rigid Motion Correction
11 (NoRMCorre), that is suitable for the registration of large scale planar or vol-
12 umetric imaging data, and we evaluate its performance against state-of-the-art
13 algorithms.

14 The general field of image registration has a long history and is still very
15 active with many different methods available. In the context of fluorescent mi-
16 croscopy time series data, an algorithm needs to be i) fast since each experiment
17 typically consists of tens of thousands of frames, ii) robust to noise arising from
18 measurement noise and neural variability/activity, and iii) able to deal with
19 non-rigid deformations that occur from natural brain movement and/or slow
20 raster scanning. In several cases rigid translation accounts for most of the mo-
21 tion and fast methods based on template alignment are often used [16, 7, 3]. For

22 dealing with non-rigid motion in the context of calcium imaging data, available
23 approaches include the work of Greenberg & Kerr [6] which is based on the
24 Lucas-Kanade method [9], Hidden Markov Models (HMM) [2, 8] approaches,
25 and block rigid registration [11].

26 NoRMCorre is based on template alignment and operates by estimating a
27 smooth non-uniform motion field that is applied into different parts of each
28 frame. Our goal is not to take a completely new approach to motion correction,
29 but rather to present and make available a robust alignment method that also
30 combines two important features:

- 31 • **Online processing:** The algorithm operates by matching patches of each
32 given frame against a template that is continuously updated based on pre-
33 viously registered frames. As such, it requires access only to the current
34 frame to be registered and the running template, plus possibly a small
35 buffer to store past templates. Consequently it is suitable for online regis-
36 tration of high volume streaming data, a useful feature that can facilitate
37 fully closed loop optical interrogation experiments [12] or compensate for
38 limited amounts of available memory.
- 39 • **Fast, non-rigid registration:** The brain is a non-rigid, non-uniformly
40 deformable medium. In modern experimental conditions, with animal
41 preparations locomoting or otherwise moving under fixed or head-mountable
42 microscopes, the brain is subject to elastic deformations. This phenomenon
43 is even more evident as equipment allows for the monitoring of increasingly
44 larger brain areas. Therefore, even when imaging at high speed correc-
45 tion of motion by rigid alignment can be inadequate. NoRMCorre splits
46 the field of view (FOV) into overlapping patches that are registered sep-
47 arately and then merged by smooth interpolation. As such it overcomes
48 the shortcomings of rigid motion alignment without a significant compu-
49 tational cost, thus remaining applicable to large scale datasets. Compared
50 to the other available non-rigid registration methods that split the FOV
51 only along one axis to capture the non-rigid motion caused by the finite

52 speed of raster scanning, NoRMCorre treats all axes uniformly aiming to
53 account for natural brain movement as well.

54 We present an application to resonant scanning two-photon microscopy data
55 and compare it against other non-rigid image registration methods in terms
56 of speed and performance. To quantify performance we propose three custom
57 metrics. Our results indicate that NoRMCorre achieves state of the art results
58 while operating at a speed not significantly slower compared to template based
59 rigid alignment.

60 **2. Materials and Methods**

61 *2.1. Algorithm Description*

62 *2.1.1. Registering a frame against a given template*

63 NoRMCorre can operate in a rigid or piecewise-rigid (pw-rigid) fashion. For
64 rigid registration, every frame is aligned against a calculated template at a sub-
65 pixel resolution using the method proposed by Guizar-Sicairos et al. [7]; the dis-
66 placement vector is computed by locating the maximum of the cross-correlation
67 between the frame and the template. The cross-correlation is efficiently ob-
68 tained via fast Fourier transform (FFT) methods, and subpixel registration is
69 achieved at a very moderate computational and memory cost by upsampling
70 the discrete Fourier transform only around the location of the maximum, and
71 then refining the translation estimate.

72 In the piecewise rigid approach, for any given frame we split the FOV into
73 a set of overlapping patches (*Fig. 1a*) according to user determined dimensions
74 and amount of overlap. Each patch is registered against the corresponding part
75 of the template at a subpixel resolution. Next, each patch is further split into
76 smaller overlapping subpatches with user-defined dimensions and amount of
77 overlap. Similarly, the computed displacement vectors for the set of the initial
78 patches are upsampled to create a smooth motion field. This associates to each
79 of the subpatches a new translation vector that is subsequently rigidly applied
80 to it (*Fig. 1b*). The registered sub-patches are then overlaid to each other and

81 in regions of overlap a weighted average is taken between all the participating
82 patches. The registered frame is also used to update the template in the online
83 scenario as discussed in the following section. A block diagram of the registration
84 pipeline is depicted in Fig. 1c.

85 *2.1.2. Updating the template*

86 The template is updated every b_w frames. Once b_w frames get registered
87 against a fixed template, their average (e.g., mean/median) is computed. These
88 averages are stored in a buffer that keeps at most the last b_p averages. The
89 new template is generated by averaging (e.g., by taking the mean/median) the
90 buffer content. Based on empirical observation, as a default choice, we use the
91 median-of-means to update the template at the end of each minibatch. The
92 template can be initialized by computing the median of the first frames (or just
93 the median of a random subset of frames).

94 *2.1.3. Online vs Offline*

95 NoRMCorre is in principle an online and one-pass algorithm since each frame
96 is registered based on the current estimate of the template. However several op-
97 timization expedients can be used to improve its performance when data and
98 memory are available. For example to avoid the influence of slow motion trends,
99 especially at the beginning of the motion correction process, we can randomly
100 permute the frames order prior to any registration, or start from the middle
101 time point of the dataset and continue outwards towards the beginning/end.
102 Moreover, when operating in offline mode, the frames within each minibatch
103 that is registered with a fixed template can be processed in parallel, leading to
104 potentially significant computational gains, depending on the available infras-
105 tructure.

106 *2.1.4. Application of the shifts*

107 Application of the computed displacement vector (shifts) is trivial when the
108 shifts are integer, since it corresponds to simple image translation and no in-
109 terpolation is required. However when fractional shifts are applied there are

110 multiple interpolation methods, based either on space interpolation (e.g., bilin-
111 ear, bicubic) or on frequency domain interpolation (FFT-based). The choice
112 of interpolation methods can lead to noticeably different results, a fact often
113 overlooked. While frequency domain methods can be slower (since they re-
114 quire the computation of an inverse FFT), they tend to preserve more structure
115 because they retain more frequency content of the signal and thus do not in-
116 troduce any smoothing effects. For example, a rigid translation corresponds to
117 a simple phase modulation in the frequency domain, which leaves invariant the
118 power spectrum density of the image. Therefore, frequency interpolation also
119 preserves the original SNR, as opposed to spatial interpolation methods that
120 smooth the signal and increase the SNR. We discuss this issue in more detail in
121 Section 3, where we show that frequency domain interpolation leads to crisper
122 image statistics compared to spatial interpolation. Since spatial smoothing can
123 also be achieved post-registration by default we use frequency domain interpo-
124 lation. To preserve the dynamic range of the original data, the registered frame
125 is restricted to take values between the minimum and maximum values of the
126 original frame.

127 *2.2. Evaluation metrics*

128 Typically motion correction algorithms for calcium imaging data are evalu-
129 ated on artificial datasets where known shifts are applied to registered data. On
130 real data, evaluation typically occurs by visual inspection, where users observe
131 the data (or a temporally downsampled version of it) before and after registra-
132 tion to assess the outcome of the registration. This makes the comparison of
133 different algorithms on real datasets very hard and biased. In this paper we
134 propose a series of simple metrics that can be used to quantify the performance
135 of different algorithms. In section 3 we show that such metrics can be important
136 for identifying locations where pw-rigid motion correction improves significantly
137 upon simple rigid registration, a task very strenuous to be performed manually.

138 *2.2.1. Correlation with the mean metric*

139 To evaluate the results of the motion correction algorithm across the differ-
140 ent frames, we use a metric that is based on the similarity (pixel-wise, Pearson’s
141 correlation coefficient r) between a reference template and each frame. For in-
142 stance, one can compute for both the raw and corrected movie the correlation
143 coefficient between each frame and the mean image across time, and then com-
144 pare them. Intuitively, an increase in the correlation coefficient for a given frame
145 indicates a better alignment with the mean¹. To account for boundary effects
146 during registration, a number of pixels around each boundary (e.g., equal to
147 the maximum shift in each direction over time) is removed when computing the
148 correlation coefficients.

149 This metric can be used to identify frames where the registration is successful
150 or not, or to compare different motion correction algorithms at the level of
151 individual frames. However, this metric critically depends on the smoothness
152 properties of each frame which, as discussed in section3, can be affected by the
153 method used to apply the computed displacements. In what follows, when using
154 this metric we compare algorithms that register frames by applying shifts with
155 the same method.

156 *2.2.2. Crispness and focus measures*

An alternative measure is to quantify how crisp is a summary image before
and after registration. This can be done by summing up the norm of the gradient
field of the image on each location. If I is the resulting summary image then
this measure of crispness can be defined as

$$c(I) = \|\|\nabla I\|\|_F, \quad (1)$$

157 where ∇ denotes the gradient vector, $|\cdot|$ denotes the magnitude, and $\|\cdot\|_F$
158 denotes the Frobenius norm. Examples of summary images include the mean

¹If a static colored channel exists, these coefficients can in principle reach values very close to one, but in practice are limited by measurement noise. For variable channels their value is also limited by the time varying courses of the underlying neuronal processes.

159 image, or the correlation image (CI)². Intuitively, a dataset with non-registered
160 motion will have a blurred mean image, resulting in a lower value for the total
161 gradient field norm. In addition to crispness, other measures of focus of the
162 summarizing image can also be used. In this case as well, we expect that spatial
163 interpolation methods can affect this measure, since introducing smoothing in
164 each frame gives rise to a smoothed, higher valued correlation image with lower
165 crispness.

166 *2.2.3. Residual motion quantification*

167 To evaluate the performance of the algorithm, we can attempt quantifying
168 motion before and after registration by using a different algorithm. In Section
169 3 we use the dense optical flow algorithm of Farnebäck [4] to estimate the resid-
170 ual motion and thus quantitatively evaluate the performance of the registration.
171 In our setting, the algorithm estimates a motion field that attempts to match
172 the current frame to the template. To do so, it relies on an efficient polyno-
173 mial approximation of pixel neighborhoods to infer locally smooth displacement
174 fields. In our hands, optical flow algorithms were particularly sensitive to the
175 low/mid-SNR conditions of typical calcium imaging datasets. Therefore, in or-
176 der to quantify the residual motion of other registration methods, the optical
177 flow algorithm needed to operate on a downsampled version of the dataset to
178 ensure robustness (and computational tractability). As such, we do not consider
179 it as an appropriate method for registering calcium imaging data, but a useful
180 and unbiased tool for assessing the performance of other methods.

181 *2.3. Technical details*

182 *2.3.1. Restricting maximum shifts*

183 To avoid potential instabilities from corrupted or very sparsely labeled frames,
184 the shifts allowed by the algorithm can be constrained within a user defined

²The image where the value for each pixel is the average of the correlation coefficients between the pixel and its neighbors.

185 region. In practice, for each frame, NoRMCorre first computes the rigid dis-
 186 placement vector for the whole frame, with a user defined maximum allowed
 187 value, e.g., $\|\mathbf{d}\|_\infty \leq M$, where \mathbf{d} is the rigid shift, M is the maximum allowed
 188 displacement in each direction, and $\|\cdot\|_\infty$ denotes the l_∞ (max) norm. Then,
 189 the displacement vector for each patch is constrained within a given region centered
 190 around the rigid displacement vector, i.e., $\|\mathbf{d}^i - \mathbf{d}\|_\infty \leq n$, where \mathbf{d}^i , is
 191 the displacement vector for patch i , and n is the maximum allowed deviation.

192 2.3.2. Merging overlapping patches

193 To apply the shifts on overlapping patches we construct a set of weight
 194 interpolating functions that are used to ensure a smooth transition between
 195 registered neighboring patches. Consider the i -th patch, centered around the
 196 point (x_i, y_i) with size (s_x, s_y) and overlap (o_x, o_y) , resulting in a total size
 197 $(s_x + 2o_x, s_y + 2o_y)$. We define the trapezoid function

$$b_X^i(x) = \begin{cases} 1, & |x - x_i| \leq s_x/2 \\ \frac{s_x + 2o_x - 2|x - x_i|}{2o_x}, & s_x/2 \leq |x - x_i| \leq s_x/2 + o_x \\ 0, & |x - x_i| > s_x/2 + o_x \end{cases}, \quad (2)$$

similarly the function $b_Y^i(\cdot)$ and the 2d function

$$B^i(x, y) = b_X^i(x)b_Y^i(y). \quad (3)$$

Then if I^1, \dots, I^K are the reconstructed patches, extended to take values in the whole FOV, the interpolated registered frame is given by

$$I(x, y) = \frac{\sum_{i=1}^K I^i(x, y)B^i(x, y)}{\sum_{i=1}^K B^i(x, y)}. \quad (4)$$

198 2.3.3. Avoiding smearing by upsampling

199 When shifts among neighboring patches differ significantly, the interpolation
 200 explained above can introduce smearing effects. Take the case of two patches
 201 overlapping along the x -direction, whose x -shifts differ by exactly 1 pixel. When

202 interpolating, the registered overlapping region will be simply a weighed aver-
203 age of two consecutive non-matching pixels along the x -direction, leading to a
204 smeared result. Upsampling to a finer grid can alleviate this undesirable out-
205 come. For example, if we up-sample the grid by a factor of 2, the difference in
206 the displacements will be 0.5 pixels, thus inducing less smearing. We empiri-
207 cally observed that smearing occurs when shifts in overlapping patches differ by
208 more than 0.5 pixels in either direction, and we suggest further upsampling to
209 prevent it.

210 In theory, the grid could be upsampled to the point where each pixel has
211 its own displacement vector. However, this approach can be computationally
212 very slow, therefore introducing a trade-off between computational efficiency
213 and smearing reduction. Hence, the upsampling factor can be chosen so that
214 it fulfills the no-smearing condition with the following formula. If n denotes
215 the maximum deviation from the rigid displacement for each patch, then two
216 neighboring patches can have displacements that differ at most $2n$ pixels in
217 each direction (an extreme case that is not expected to be encountered often
218 in practice), and an upsampling factor of $2^{2+\lceil \log_2 n \rceil}$, where $\lceil x \rceil$ denotes the
219 minimum integer greater or equal to x , guarantees the no smearing condition.
220 For computational reasons, in practice we often use a smaller factor, and the
221 interpolation is avoided for the frames where the smearing condition is not
222 satisfied.

223 *2.3.4. Choosing patch size and amount of overlap*

224 Our algorithm requires a template with strong reference points that facili-
225 tates robust matching and alignment. When splitting into patches to perform
226 pw-rigid motion correction, each patch (together with its overlap) needs to con-
227 tain enough signal to produce a clear template. In dark areas, for instance, it
228 is difficult to find bright reference points and the alignment consequently fails.
229 Empirically, for a typical 512×512 FOV with somatic imaging, an initial patch
230 size of 128×128 (with additional 32 pixels of overlap in each direction) is a
231 good choice. However, if the labelling is sparse then either a larger patch size

232 and/or overlap might be required to ensure there is enough information for
233 robust template alignment.

234 The amount of overlap between subpatches ensures a smooth interpolation
235 between neighboring patches and alleviates boundary effects during the FFT
236 registration. If l is the size of the initial patch along one dimension, u is the
237 upsampling factor, and $M + n$ is the allowed maximum displacement (maximum
238 rigid displacement plus deviation), then we choose the overlap after upsampling
239 to be larger than $M + n - l/u$, to ensure that each patch is not shifted by an
240 amount larger than its dimension.

241 *Software*

242 Matlab code (also applicable to 3D volumetric imaging data) is available
243 as a standalone package <https://github.com/simonsfoundation/NoRMCorre>.
244 This package complements and will be integrated with the CNMF Matlab
245 package for demixing and deconvolution of registered movies [13] available at
246 https://github.com/epnev/ca_source_extraction. NoRMCorre is also im-
247 plemented in Python <https://github.com/simonsfoundation/CaImAn> as part
248 of the CaImAn package [5].

249 **3. Results**

250 We tested the algorithm on data collected *in vivo* with a two-photon mi-
251 croscope on a mouse expressing GCaMP6f in the parietal cortex, courtesy of
252 S.A. Koay and D. Tank (Princeton University). The FOV had size 512×512
253 pixels and the data was acquired at 30Hz. Fig. 2 provides a demonstration
254 of the performance of the rigid and piecewise rigid versions of our algorithm
255 with respect to the various proposed metrics on a 2000 frame segment of the
256 dataset. According to all the considered metrics, pw-rigid motion correction
257 led to improved registration compared to plain rigid motion correction, which
258 in turn improved significantly over the non-registered data. Fig. 2A shows a
259 100×100 pixel patch of the resulting mean for raw, rigid and pw-rigid cor-
260 rected. By inspection, the pw-rigid correction preserves more fine structure,

261 something that is also captured by the crispness metric (see eq. (1)) producing
262 values of 4.3×10^3 , 6.69×10^3 , and 7.35×10^3 for raw, rigid and piecewise-
263 rigid respectively. The same trend is also observed for the correlation with the
264 mean metric (*Fig. 2b*) and the average per frame optical flow metrics (*Fig. 2c*),
265 where the scatter plots demonstrate that the pw-rigid correction improves over
266 the plain rigid correction for nearly all 2000 frames. Consistently, the optical
267 flow metric shows that the improvement is also global in space (every region of
268 the FOV exhibits less movement), with most of the remaining movement esti-
269 mated to be around the boundaries and due to poorer SNR or other possible
270 border effects (*Fig. 2e*). *Fig. 2d* shows the displacements along the x -axis for
271 a small segment of frames (black), plotted against the displacements for each
272 of the different patches (before upsampling). Connecting with *Fig. 2b,c* left,
273 we notice that pw-rigid motion correction brings the most additional benefits
274 over rigid motion correction when the dispersion of the displacements over the
275 different patches is high, i.e., NoRMCorre estimates and corrects for a higher
276 amount of non-rigid motion. The results are better displayed in movie format.
277 Supplemental Movie 1 demonstrates the large variety of motion field patterns
278 the algorithm estimates during the registration process. Supplemental Movie 2
279 shows a downsampled version of the results of rigid and pw-rigid registration,
280 alongside the original data.

281 Next we compared NoRMCorre in its Python implementation with i) a Hid-
282 den Markov Model based algorithm [2], as implemented in the Python package
283 SIMA [8], ii) the block-rigid approach of the Matlab package Suite2p [11], and
284 iii) the Lucas-Kanade approach of Greenberg & Kerr [6]. These three methods
285 are also suitable for non-rigid motion correction and have available implementa-
286 tions in Python (SIMA) or Matlab (Suite2p, Lucas-Kanade). We compared the
287 three methods with respect to the quality metrics and the speed. For reference
288 we also include the metrics of the non-registered data as well as the performance
289 of rigid motion correction from the Python implementation of NoRMCorre. The
290 results (*Table 1*) indicate that NoRMCorre achieves the best performance for
291 crispness metrics and residual motion at a speed comparable to rigid motion

2000 frames	Crisp (mean, a.u.)	Crisp (CI)	Optical Flow (RMS, pixels)	Time (sec)	Interp. Interp.
Original	4301	9.87	1.574 ± 1.502	–	–
Rigid	6690	10.98	0.443 ± 0.328	40	FFT
SIMA	6678	9.25	0.244 ± 0.082	530	Integer
Suite2p	6694	9	0.246 ± 0.08	86	FFT
Lucas-Kanade	6394	10.36	0.197 ± 0.084	1856	Bilinear
NoRMCorre	7483	10.69	0.154 ± 0.09	89	Bicubic
NoRMCorre	7531	11.48	0.15 ± 0.09	117	FFT

Table 1: Comparison of NoRMCorre with other non-rigid motion correction algorithm on a 2000 frame, 512×512 pixel *in vivo* mouse cortex dataset.

292 correction, which is unsurprisingly the fastest method but produces the worst
 293 results in terms of residual motion. The residual motion was calculated with
 294 the dense optical flow (OF) algorithm of Farnebäck [4] in its OpenCV (v3.2,
 295 <http://opencv.org>) implementation, after temporal downsampling of the data
 296 to increase the SNR (see Section 2.2.3). We note that for all of the other three
 297 different methods, the best and reported results were obtained by taking blocks
 298 along the x -direction which is parallel to the raster scanning direction, demon-
 299 strating the fact that the largest part of the motion may not be due to raster
 300 scanning effect. Details of the various implementations are given in the supple-
 301 ment.

302 Table 1 also illustrates the effect of the interpolation method. When apply-
 303 ing NoRMCorre with bicubic interpolation it achieves similar residual motion
 304 compared to NoRMCorre with Fourier interpolation albeit at a faster speed.
 305 However, the crispness of the mean and correlation images decreases due to the
 306 smoothness introduced by the bicubic interpolation. This point is highlighted
 307 even further in Fig. 3, where the correlation and mean images are shown for
 308 NoRMCorre and the Lucas-Kanade method, emphasizing the effect of differ-

309 ent interpolation methods. Bilinear and bicubic interpolation smooths the data
310 (*Fig. 3A, left and middle*), and biases upwards the correlation between neigh-
311 boring pixels, as opposed to Fourier interpolation that retains the structure
312 displayed by the weak correlations between neighboring pixels (*Fig. 3A, right*).
313 On the other hand, the effect on the correlation with the mean metric is opposite
314 leading to higher values for bilinear interpolation with Lucas-Kanade registra-
315 tion (0.499 ± 0.033), and bicubic interpolation with NoRMCorre registration
316 (0.443 ± 0.017), as opposed to Fourier based interpolation with NoRMCorre
317 which achieves a significantly lower value (0.399 ± 0.014). This highlights the
318 sensitivity of this metric on the interpolation method, and why it should be
319 used carefully in comparisons.

320 **4. Discussion**

321 Non-rigid motion within a frame can occur not only due to slow raster scan-
322 ning but also because of relative brain elastic deformation within the field of
323 view. While faster raster scanning can result in higher imaging rates for a given
324 FOV and thus reduce the amount of intra frame motion, modern methods enable
325 imaging of even larger areas and/or volumes (e.g., Sofroniew et al. [14], Stirman
326 et al. [15]) within which significant intra-frame motion is still possible. We be-
327 lieve that fast non-rigid motion correction will remain an important challenge
328 in the future. NoRMCorre provides a simple and online method based on piece-
329 wise rigid template alignment that achieves state of the art results at a speed
330 comparable to real time.

331 To better quantify the benefits of piecewise registration over rigid registra-
332 tion as well as to compare NoRMCorre with other non-rigid motion registration
333 algorithms we developed some intuitive metrics that measure the crispness of
334 the registered images and also used independent algorithms to estimate the
335 amount of residual motion after registration. These metrics also highlighted
336 the importance of the interpolation method that is chosen to apply the com-
337 puted displacement vectors. While the effect of the smoothing introduced by the

338 spatial interpolation methods might be minimal, and actually create the per-
339 ception of a higher SNR, we took the stand that the statistics of the registered
340 data should reflect the original input as much as possible, spatial smoothing can
341 occur downstream in the analysis when necessary. We argued that by using the
342 computationally more expensive Fourier based interpolation and avoiding any
343 smoothing, one can better preserve the statistics of originally acquired data.

344 The ultimate goal of motion registration is to stabilize the FOV. This is
345 important for segmentation reasons because several current source extraction
346 methods identify sources by searching for groups of pixels that behave similarly
347 with each other across time [13]. An alternative to such approaches would
348 be to track individual neurons over time, an approach that has been taken
349 when imaging freely moving *C. elegans* [10], where the deformations can be very
350 dramatic. However, these methods tend to be computationally very expensive
351 and have not yet found applications in registering other types of data.

352 The dataset used as an example in this paper pertains to two-photon, two-
353 dimensional, raster scanning imaging of mostly cell bodies. However, our ap-
354 proach can also be applied to other types of imaging datasets. For the case
355 of one-photon, microendoscopic data, high pass spatial filtering can be used to
356 remove the bulk of the smooth background signal created by the large integra-
357 tion volume, and create stark reference points, prior to applying registration.
358 NoRMCorre can also be readily applied to dense volumetric data (e.g., SCAPE
359 microscopy [1]), where non-rigid motion can exist in all 3 directions. More
360 details about such applications will be presented in the future.

361 **Acknowledgments**

362 We thank D. Chklovskii, J. Magland (Flatiron Institute, Simons Founda-
363 tion), J. Gauthier, S.A. Koay (Princeton University) and N. Sofroniew (Janelia
364 Research Campus) for useful discussions. We thank S.A. Koay and D. Tank
365 (Princeton University) for providing us with the *in vivo* mouse cortex dataset.

366 **References**

- 367 [1] Bouchard, M. B., Voleti, V., Mendes, C. S., Lacefield, C., Grueber, W. B.,
368 Mann, R. S., Bruno, R. M., & Hillman, E. M. (2015). Swept confocally-
369 aligned planar excitation (sape) microscopy for high-speed volumetric
370 imaging of behaving organisms. *Nature photonics*, *9*, 113–119.
- 371 [2] Dombek, D. A., Khabbaz, A. N., Collman, F., Adelman, T. L., & Tank,
372 D. W. (2007). Imaging large-scale neural activity with cellular resolution
373 in awake, mobile mice. *Neuron*, *56*, 43–57. URL: [http://dx.doi.org/10.](http://dx.doi.org/10.1016/j.neuron.2007.08.003)
374 [1016/j.neuron.2007.08.003](http://dx.doi.org/10.1016/j.neuron.2007.08.003). doi:10.1016/j.neuron.2007.08.003.
- 375 [3] Dubbs, A., Guevara, J., & Yuste, R. (2016). moco: Fast motion correction
376 for calcium imaging. *Frontiers in neuroinformatics*, *10*.
- 377 [4] Farnebäck, G. (2003). Two-frame motion estimation based on polynomial
378 expansion. In *Scandinavian conference on Image analysis* (pp. 363–370).
379 Springer.
- 380 [5] Giovannucci, A., Friedrich, J., Deverett, B., Staneva, V., Chklovskii, D., &
381 Pnevmatikakis, E. (2017). Caiman: An open source toolbox for large scale
382 calcium imaging data analysis on standalone machines. In *Computational*
383 *and Systems Neuroscience Meeting, Cosyne*.
- 384 [6] Greenberg, D. S., & Kerr, J. N. (2009). Automated correction of fast motion
385 artifacts for two-photon imaging of awake animals. *Journal of neuroscience*
386 *methods*, *176*, 1–15.
- 387 [7] Guizar-Sicairos, M., Thurman, S. T., & Fienup, J. R. (2008). Efficient
388 subpixel image registration algorithms. *Optics letters*, *33*, 156–158.
- 389 [8] Kaifosh, P., Zaremba, J. D., Danielson, N. B., & Losonczy, A. (2014).
390 SIMA: Python software for analysis of dynamic fluorescence imaging data.
391 *Front Neuroinform*, *8*.

- 392 [9] Lucas, B. D., Kanade, T. et al. (1981). An iterative image registration
393 technique with an application to stereo vision. In *IJCAI* (pp. 674–679).
394 volume 81.
- 395 [10] Nguyen, J. P., Linder, A. N., Plummer, G. S., Shaevitz, J. W., & Leifer,
396 A. M. (2016). Automatically tracking neurons in a moving and deforming
397 brain. *arXiv preprint arXiv:1610.04579*, .
- 398 [11] Pachitariu, M., Stringer, C., Schröder, S., Dipoppa, M., Rossi, L. F., Caran-
399 dini, M., & Harris, K. D. (2016). Suite2p: beyond 10,000 neurons with
400 standard two-photon microscopy. *bioRxiv*, (p. 061507).
- 401 [12] Packer, A. M., Russell, L. E., Dagleish, H. W., & Häusser, M. (2015). Si-
402 multaneous all-optical manipulation and recording of neural circuit activity
403 with cellular resolution in vivo. *Nature Methods*, *12*, 140–146.
- 404 [13] Pnevmatikakis, E. A., Soudry, D., Gao, Y., Machado, T. A., Merel, J.,
405 Pfau, D., Reardon, T., Mu, Y., Lacefield, C., Yang, W. et al. (2016).
406 Simultaneous denoising, deconvolution, and demixing of calcium imaging
407 data. *Neuron*, *89*, 285–299.
- 408 [14] Sofroniew, N. J., Flickinger, D., King, J., & Svoboda, K. (2016). A large
409 field of view two-photon mesoscope with subcellular resolution for in vivo
410 imaging. *eLife*, *5*:e14472.
- 411 [15] Stirman, J. N., Smith, I. T., Kudenov, M. W., & Smith, S. L. (2016). Wide
412 field-of-view, multi-region, two-photon imaging of neuronal activity in the
413 mammalian brain. *Nature Biotechnology*, .
- 414 [16] Thevenaz, P., Ruttimann, U. E., & Unser, M. (1998). A pyramid approach
415 to subpixel registration based on intensity. *IEEE transactions on image*
416 *processing*, *7*, 27–41.

417 **Figures**

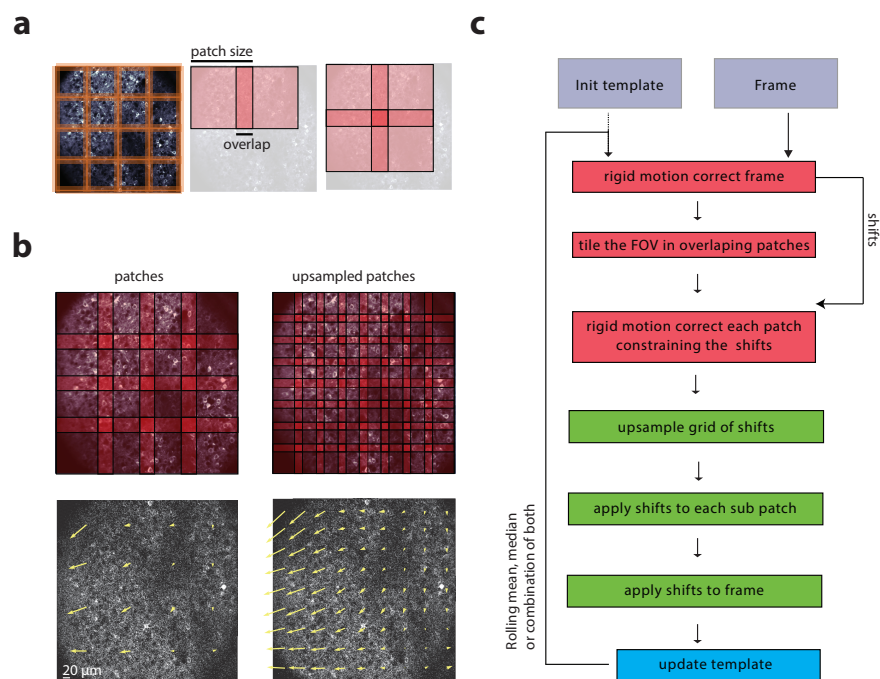


Figure 1: **Schematic representation of the proposed algorithm.** *a*: Illustration of the scheme used to overlap patches. *b*: *Top*. Illustration of the process of upsampling the shifts. *Bottom*. Visual representation of the motion estimated field on the original (left) and upsampled (right) patches. The yellow arrow's length represent the direction and magnitude of the motion field. *c*: Pipeline for piece-wise rigid registration of a frame against a given template, and template updating.

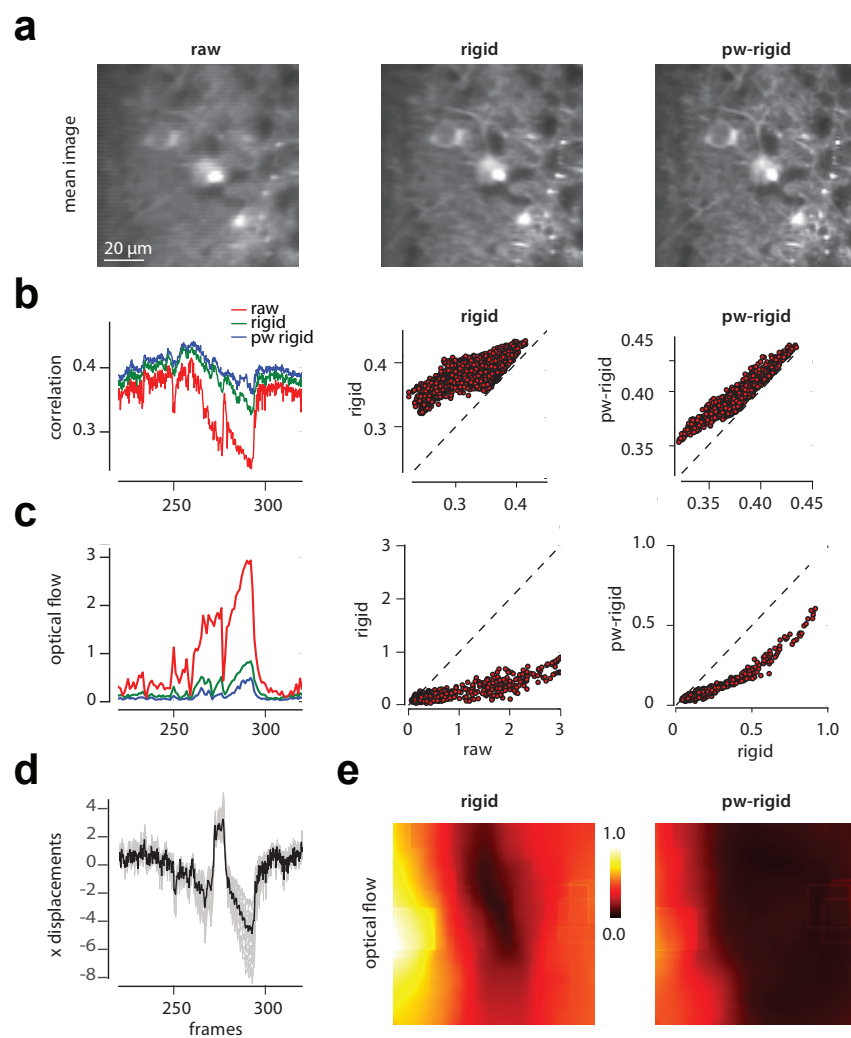


Figure 2.

Figure 2: **Illustration of performance on *in vivo* mouse parietal cortex data.** *a*: Mean image of raw data (focused on a 100×100 pixels part of the FOV for clarity). Raw data (*left*), rigid corrected (*middle*) and piecewise-rigid corrected (*right*). NoRMCorre with pw-rigid correction results in a more structured mean image as quantified by the crispness of the image (1) ($c(\text{raw}) = 4.3 \times 10^3$, $c(\text{rigid}) = 6.69 \times 10^3$, $c(\text{piecewise}) = 7.53 \times 10^3$, measurements in absolute units). *b*: Quantification of performance based on the correlation with mean metric. For nearly every frame rigid correction improves over the raw data, and pw-rigid improves over rigid. *Left*. Mean correlation metric for a subset of frames. Scatter plot of frame-by-frame mean correlation metric of raw vs rigid (*center*) and rigid vs pw-rigid (*right*). *c*, *e*: Quantification of performance using the optical flow measure averaged over space (*c*, mean over space RMS value in pixels) and over time (*e*, mean over time RMS value of residual motion in pixels). Consistently, pw-rigid correction improves over plain rigid correction (*left*, frame by frame; *center*, scatter raw vs rigid; *right*, scatter rigid vs pw-rigid) and most of the remaining motion, as estimated with optical flow, remains on the boundaries of the FOV (*e*, *left*). *d*: Comparison of the rigid displacement (black) along the x-axis with the displacement of each patch for a subset of frames. The main benefits from the piecewise rigid correction, as can be seen from b and c (*left*) come at frames where the displacements exhibit maximum dispersion.

418

419

420

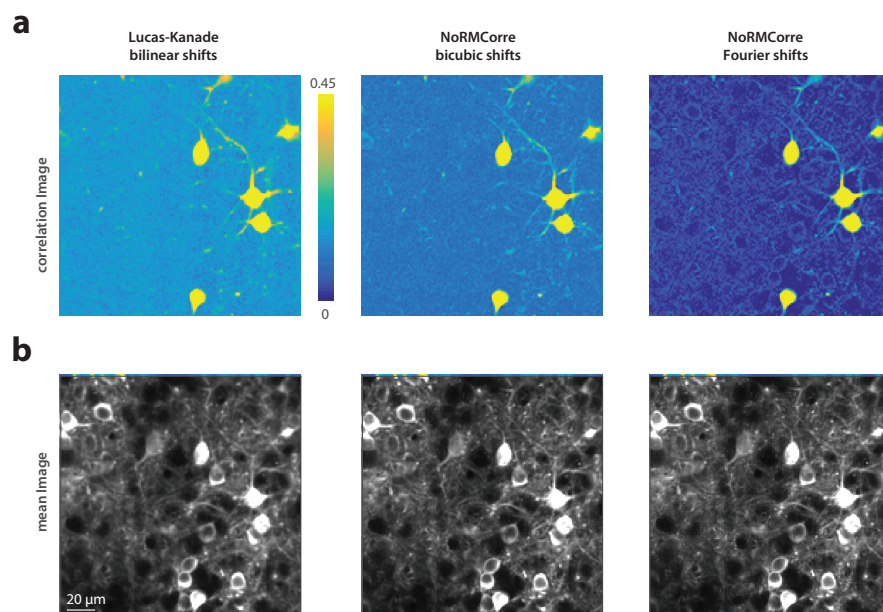


Figure 3: **Effect of interpolation method on registered data.** *a*: Correlation images for registered methods with 3 different methods restricted on a 170×170 pixels part of the FOV. Lucas-Kanade method with bilinear interpolation (*left*), and NoRMCorre with bicubic interpolation (*middle*) and Fourier interpolation (*right*). Fourier interpolation retains the weak correlation structure between neighboring pixels, whereas spatial interpolation “washes” away this structure by introducing smoothing during the shift application resulting in higher values for the correlation image. *b*: Mean images for the three approaches. The differences are less visible by eye, but quantitatively NoRMCorre with Fourier interpolation produced the crispest mean image (see *Table 1*).

422 **Supplemental Material**

423 *Dataset description*

424 Data was obtained from the parietal cortex of a transgenic GCaMP6f-expressing
425 mouse during a behavioral task. Field of view was approximately $500 \times 500 \mu\text{m}^2$
426 (512 by 512 pixels) in size and at depth $125 \mu\text{m}$ below the dura surface. Horizon-
427 tal scans of the laser were performed using a resonant galvanometer, resulting
428 in a frame acquisition rate of 30Hz .

429 *Implementation details*

430 All analysis and simulations were performed on a Dell Precision Tower 7910,
431 24 cores Intel(R) Xeon(R) E5-2643 v3 @3.40 GhZ, 128 GB RAM). For the pw-
432 rigid algorithm, the FOV was initially split in patches of size 128×128 pixels
433 with an additional 32 pixels of overlap on each side. Each patch was further
434 upsampled by a factor of 4. The algorithm was run in its offline mode with
435 template obtained from the rigid registration of the first 500 frames. For the
436 other three methods (SIMA, Suite2p, Lucas-Kanade), best results were obtained
437 by taking blocks of size 512×16 pixels (excluding overlap), tiled horizontally (in
438 parallel and not vertical to the raster scanning direction). For computation of
439 the various metrics 12 pixels were removed from each side along both directions
440 to avoid the boundary effects due to the registration. The optical flow algorithm
441 was applied to a $5 \times$ downsampled version of the registered data to increase SNR
442 and robustness.

443 *Description of Supplemental Movies*

444 *Supplemental Movie 1. Depiction of the online pw-rigid motion correction proce-*
445 *dure:.* Each frame of the original data (*top left*) is registered against a template
446 (*bottom right*) in a piecewise rigid manner by shifting small patches according
447 to the computed and upsampled motion field (*bottom left*). The resulting reg-
448 istered frame is shown on top right. Observance of the motion field shows the
449 diverse non-rigid motion patterns that the algorithm estimates along both di-
450 rection. The template is updated online during the registration process every

451 50 time steps. The movie is reproduced at the original data acquisition rate of
452 30 Hz.

453 *Supplemental Movie 2. NoRMCorre corrects for non rigid motion along both*
454 *directions.. Comparison between the original data (left), corrected with rigid*
455 *registration (middle) and piecewise rigid registration with NoRMCorre (right).*
456 Original and registered datasets are first downsampled $5\times$ in time and then
457 reproduced at $3\times$ the original rate to aid the visual perception of the registration
458 results. NoRMCorre with pw-rigid registration performs significantly better
459 compared to rigid registration.